Physics of Plasmas

RESEARCH ARTICLE | MAY 11 2023

Toward using collective x-ray Thomson scattering to study C–H demixing and hydrogen metallization in warm dense matter conditions

D. Ranjan ✉; K. Ramakrishna; K. Voigt; ... et. al

Physics of Plasmas 30, 052702 (2023)
https://doi.org/10.1063/5.0146416

Physics of Plasmas ARTICLE pubs.aip.org/aip/php

Toward using collective x-ray Thomson scattering to study C–H demixing and hydrogen metallization in warm dense matter conditions

Cite as: Phys. Plasmas **30**, 052702 (2023); doi: 10.1063/5.0146416
Submitted: 13 February 2023 · Accepted: 23 April 2023 ·
Published Online: 11 May 2023

D. Ranjan,[1,2,a)] K. Ramakrishna,[3] K. Voigt,[1,4] O. S. Humphries,[1,5] B. Heuser,[1,2] M. G. Stevenson,[2] J. Lütgert,[2] Z. He,[1,2,6] C. Qu,[2] S. Schumacher,[2] P. T. May,[2] A. Amouretti,[7] K. Appel,[5] E. Brambrink,[5] V. Cerantola,[5] D. Chekrygina,[8] L. B. Fletcher,[9] S. Göde,[5] M. Harmand,[7] N. J. Hartley,[9] S. P. Hau-Riege,[10] M. Makita,[5] A. Pelka,[1] A. K. Schuster,[1,4] M. Šmíd,[1] T. Toncian,[1] M. Zhang,[1,11] T. R. Preston,[5] U. Zastrau,[5] J. Vorberger,[1] and D. Kraus[1,2,b)]

AFFILIATIONS

[1]Helmholtz-Zentrum Dresden-Rossendorf, Bautzner Landstraße 400, 01328 Dresden, Germany
[2]Institut für Physik, Universität Rostock, 18051 Rostock, Germany
[3]Center for Advanced Systems Understanding (CASUS), Helmholtz-Zentrum Dresden-Rossendorf (HZDR), 02826 Görlitz, Germany
[4]Technische Universität Dresden, 01069 Dresden, Germany
[5]European XFEL, 22869 Schenefeld, Germany
[6]Shanghai Institute of Laser Plasma, 201800 Shanghai, China
[7]Sorbonne Université, Muséum National d'Histoire Naturelle, UMR CNRS 7590, Institut de Minéralogie, de Physique des Matériaux, et de Cosmochimie (IMPMC), F-75005 Paris, France
[8]Scientific Computing Department, Rutherford Appleton Laboratory, Science and Technology Facilities Council, Harwell Campus, Didcot OX11 0QX, United Kingdom
[9]SLAC National Accelerator Laboratory, Menlo Park, California 94309, USA
[10]Lawrence Livermore National Laboratory, Livermore, California 94550, USA
[11]Institute of Physical Science and Information Technology, Anhui University, Hefei 230601, China

[a)]**Author to whom correspondence should be addressed:** d.ranjan@hzdr.de
[b)]**Electronic mail:** dominik.kraus@uni-rostock.de

ABSTRACT

The insulator–metal transition in liquid hydrogen is an important phenomenon to understand the interiors of gas giants, such as Jupiter and Saturn, as well as the physical and chemical behavior of materials at high pressures and temperatures. Here, the path toward an experimental approach is detailed based on spectrally resolved x-ray scattering, tailored to observe and characterize hydrogen metallization in dynamically compressed hydrocarbons in the regime of carbon–hydrogen phase separation. With the help of time-dependent density functional theory calculations and scattering spectra from undriven carbon samples collected at the European x-ray Free-Electron Laser Facility (EuXFEL), we demonstrate sufficient data quality for observing C–H demixing and investigating the presence of liquid metallic hydrogen in future experiments using the reprated drive laser systems at EuXFEL.

I. INTRODUCTION

The first confirmed discovery of an exoplanet in 1992[1] and then the discovery of an exoplanet around a Sun-like star by Mayor and Queloz[2] opened the floodgates for the detection of exoplanets, leading to multiple dedicated missions to look for exoplanets across the galaxy. After 30 years and over 5000 confirmed exoplanets,[3] it is now increasingly important to understand how planetary systems form and evolve. A large number of discovered exoplanets lie in the range of

masses of gas giants like Jupiter and Saturn and ice giants like Uranus and Neptune, with the ice giants dominating the population.[4,5] Studying these large bodies in our Solar System continues to enhance our understanding of the formation and evolution of planetary systems in general.

Various probe missions afforded us extensive data and improved our understanding of the planets by exploring the upper layers and space around them. The interiors of these astrophysical bodies can be constrained using the measurements of their physical properties, but establishing the internal structure and their bulk composition requires a better understanding of the behavior of the chemical species at high-pressure and high-temperature conditions. The thermal energies at planetary interior conditions are at the same order of magnitude as the energies stored in the chemical bonds, resulting in expected complex chemical processes including phase transitions, species separation, and demixing.[6,7] The chemical composition and potential chemical processes taking place inside these planets are essential for creating better models and understanding their thermal, magnetic, and electrical properties.[8]

The deep planetary conditions are at the low-temperature end of the warm dense matter (WDM) regime. WDM describes the transition region between cold condensed matter and high-temperature plasmas.[9,10] One of the materials with great interest in research at WDM conditions is metallic hydrogen. It was first predicted by Wigner and Huntington[11] that solid molecular hydrogen would transform into metal at high pressures. A pressure-induced liquid–liquid phase transition from molecular hydrogen to a metallic phase is relevant to planetary interiors and therefore has been widely researched.[12–14] The transition is referred to as plasma phase transition, which, depending on temperature, is predicted to either be an abrupt first-order phase transition or a continuous transition to the metallic state.[15–17]

Theoretical and experimental studies of metallic hydrogen have significantly contributed to the current understanding of planetary evolution. Jupiter and Saturn are predicted to have an interior dominated by liquid metallic hydrogen, which is in contrast to the properties of the insulating, molecular form present in the outer layers.[6] This highly condensed metallic hydrogen in the interior of gas giant planets is expected to be responsible for the strong dynamo that drives their exceptionally strong magnetic fields.[18] Uranus and Neptune are most often modeled to be made of three layers: a rocky core consisting of silicates and iron, an "icy" shell that contains a mixture of water, methane, and ammonia, and a gaseous envelope dominated by hydrogen and helium.[19–21] In the high-pressure and high-temperature environment of these icy-giant planets, it is predicted that methane will form polymeric hydrocarbon chains[8,22] and, deeper toward the core, will dissociate into carbon in the form of diamond and metallic hydrogen.[23–26]

Transcribing the physics of WDM state requires consideration of highly interacting particles. Coupling and quantum effects are not perturbations in the WDM regime, but are as strong as the thermal energy. The complex interplay of competing forces is a reason that the precise theoretical modeling to adequately portray the physics is very difficult.[9,27,28] To test the models, dedicated laboratory experiments need to be performed. The so-far applied experimental methods are mostly based on cryogenic liquid hydrogen as the initial material and include static compression approaches using diamond anvil cells[29–32] and various dynamic compression techniques.[15,33–36]

In addition to the challenges of compressing hydrogen to metallization conditions using the above-mentioned methods, the complexity of cryogenic sample environments to start with high-density hydrogen from the beginning also limits diagnostic capabilities. The measurement of electrical conductivities for liquid H_2 and D_2 dynamically compressed by high-velocity impactors driven by a gun has provided the first pioneering insight.[35] In more recent approaches, the insulator–metal transition of hydrogen has been characterized by determining the surface reflectivity of the compressed sample. While there has been progress using a surface reflectivity method, there are notable discrepancies in the P–T conditions where hydrogen metallization was observed.[33,34] Indeed, systematic uncertainties of the approach arise from the fact that the reflecting interface is often in direct contact with a material containing the sample, which may induce additional chemistry and changes in the electronic structure. Therefore, techniques capable of accessing the interior of the sample and probing the bulk volume are preferable but difficult to realize experimentally. The high electronic densities of WDM make it opaque to optical probes, and therefore, hard x-rays of keV energy are required to access the bulk volume.

As a further development of pioneering experiments using laser-based x-ray sources, the advent of x-ray free-electron lasers has matured enough to provide revolutionary capabilities in the diagnosis of dynamically compressed matter, mainly created by high energy lasers producing compression waves on nanosecond timescales. Methods applied include spectrally resolved x-ray Thomson scattering (XRTS) that can access the electron temperature and density, the ionization state, and plasmon features. The plasmon feature is sensitive to frequency-dependent electron–ion collision processes, which are related to the electrical conductivity.[37]

In this work, we present high-resolution x-ray scattering measurements obtained in the collective regime from undriven carbon samples in comparison with theoretical predictions using the time-dependent density functional theory (TDDFT).[38] Furthermore, the possibility of observing the C–H demixing and hydrogen metallization via plasmon scattering under high pressure and high temperature is investigated with the help of experiments including a rep-rated energetic shock driver.

II. X-RAY THOMSON SCATTERING

X-ray Thomson scattering is an established diagnostic method for characterizing WDM.[39,40] The particular experimental setup used illuminated sample by a linearly polarized x-ray free-electron laser in the horizontal plane. The incident wave vector $\mathbf{k_0}$ is described with $k_0 = 2\pi E_0/hc$. The scattered radiation is observed at the scattering angle θ along the direction of the scattered wave vector $\mathbf{k_S}$ above the sample by a spectrometer. The scattering vector $\mathbf{k}$ is defined by $\mathbf{k} = \mathbf{k_S} - \mathbf{k_0}$. For small momentum and energy transfers from the incident x-ray photon to the electron ($\hbar\omega \ll \hbar\omega_0$, where ω_0 denotes the frequency of the incident radiation), the magnitude of the incident wave vector is close to the scattered wave vector, $k_0 \approx k_s$, and the absolute value of the scattering vector k can be determined by

$$k = |\mathbf{k}| = 4\pi \frac{E_0}{hc} \sin\left(\frac{\theta}{2}\right). \quad (1)$$

The collective and non-collective regimes are distinguished by the scattering parameter $\alpha = 1/k\lambda_S$, where λ_S is the plasma screening

length: $\alpha \gtrsim 1$ corresponds to the collective scattering regime, and $\alpha \ll 1$ is characteristic for non-collective scattering. As α is dependent on k, different regimes can be accessed by varying the incident x-ray energy E_0 and/or the scattering angle θ. Here, the focus is on collective scattering to resolve plasmon oscillations of the electrons.

The obtained spectra can, then, be compared to models of the dynamic structure factor $S(k, \omega)$, which describes the scattering of radiation from charge density fluctuations. Theoretically, the dynamic structure factor can be obtained by the inversion of the total electronic dielectric function $\epsilon(\mathbf{k}, \omega)$. This expression is equivalent to the total electron density response function $\chi(\mathbf{k}, \omega)$.[41] The dynamic structure factor is obtained using the fluctuation–dissipation theorem,[42]

$$S(\mathbf{k}, \omega) = \frac{\hbar}{\pi n_e} \frac{1}{1 - e^{\hbar\omega/k_B T_e}} \mathrm{Im}[\chi(\mathbf{k}, \omega)]. \quad (2)$$

For an advanced study of the sample properties, dynamic structure factor predictions can be extracted from state-of-the-art *ab initio* methods. For the study, time-dependent density functional theory (TDDFT) simulations[43] were performed. At ambient conditions, the linear-response TDDFT calculations were performed using the full-potential linearized augmented-plane wave code implemented in Elk[44] using bootstrap,[45] a long-range exchange-correlation (XC) kernel for TDDFT as implemented in the Elk code. The response functions at high-pressure and high-temperature conditions are evaluated using the adiabatic local density approximation for TDDFT in yambo[46] applying the Kohn–Sham[47] orbitals evaluated by Quantum ESPRESSO.[48] The simulations were performed for a system size ranging from 64 to 256 atoms consisting of C, H, CH, CH_3, and C_3H in a supercell using a $2 \times 2 \times 2$ k-point mesh. The Perdew–Burke–Ernzerhof (PBE)[49] XC functional is used in all the calculations.

III. RESULTS

The experimental data presented here were obtained at the High-Energy-Density (HED) instrument of the European X-ray Free-Electron Laser Facility (EuXFEL).[50] The setup used was typical for *in situ* x-ray diagnostics of laser-driven shock waves at XFEL facilities combining spectrally resolved x-ray scattering in both forward and backward geometries with x-ray diffraction, and only the drive laser was not yet available. The details of the setup together with an analysis of the backward scattering data have been described by Voigt *et al.*[51] For demonstrating the forward scattering capabilities, 10 μm thick diamond samples were probed by x-ray pulses with a photon energy of ~6000 eV, focused to <10 μm spot sizes using beryllium compound refractive lenses. A monochromator was used to reduce the energy bandwidth to ~1 eV, from originally ~20 eV corresponding to the self-amplified spontaneous-emission (SASE) bandwidth. Both the spectrometers used cylindrically bent Highly Annealed Pyrolytic Graphite (HAPG) crystals with 80 mm radius of curvature, albeit the crystals used in the forward scattering setups had coating thickness of 100 μm compared with 40 um in the backward direction.[52] The backward scattering setup had a JUNGFRAU detector[53] at 155, to study x-ray Raman spectroscopy from different samples.[51] The forward scattering signal was collected on an ePix100 detector[54] at 18. Dark images were taken as an average of 1200 frames (corresponding to a 2 min 10 Hz acquisition) per gain mode. The setup also included an ePix100 detector for x-ray diffraction (XRD) and an Andor Zyla 5.5 sCMOS detector along with a bent Si-111 crystal spectrometer downstream of transmitted x-rays to measure the source spectrum.[51]

For the analysis of the forward spectrometer, pixel values with less than a nominal threshold associated with a clear single photon hit were truncated to zero for reducing the noise. Pixel noise in high gain corresponds to ~290 eV, allowing us to identify single photon counts with only Poisson noise. Several thousand two-dimensional detector images were, then, summed up to derive a lineout. Figure 1 illustrates the forward scattering spectrum from a 10 μm thick diamond sample. The plasmon feature, in this case collective excitations of valence band electrons, is usually downshifted by ~30 eV with respect to the elastic peak.[55] Using the monochromator allows the plasmon feature and the substructures to be clearly resolved, which would have been smeared out with pure SASE.

The forward scattering angle and the XFEL photon energy result in an absolute value of the scattering vector of ~0.94 $Å^{-1}$ applying Eq. (1). This wave number was, then, used as input for generating synthetic spectra from TDDFT simulations. In Fig. 2, the plasmon feature obtained from the experiment is compared with the TDDFT simulations convolved with the experimental instrument function. The synthetic spectrum shows reasonable agreement with the experimental data, reproducing the detailed features, except the surface plasmon feature at ~25 eV,[56] which is not covered by the bulk nature of the simulations. The total energy resolution obtained using the monochromator with 100 μm HAPG crystals is ~5 eV. As the 100 μm HAPG crystals have more depth broadening than the 40 μm HAPG crystals that were used in the backward scattering setup of the same experiment, by using the 40 μm HAPG crystals in the forward scattering setup could bring down the total spectral resolution to ~3 eV.[52] Solely using the SASE mode results in ~20 eV, which smears out all substructures of the plasmon feature and results in overlap with the elastic scattering peak. The lower signal due to the monochromator has been compensated by taking a larger number of shots cumulatively.

IV. DISCUSSION

The obtained results suggest the applicability of the method presented for observing C–H demixing and hydrogen metallization under

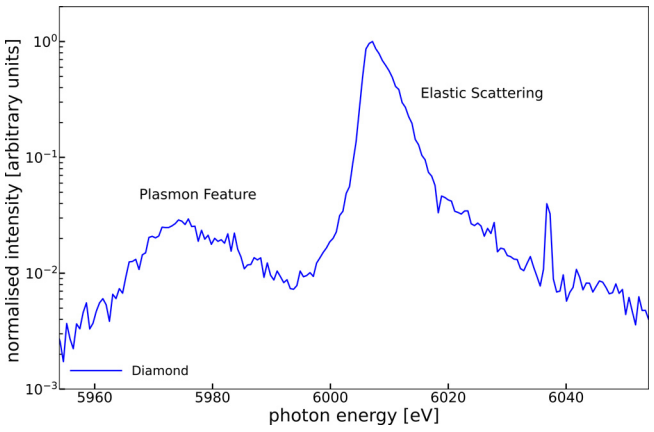

FIG. 1. Forward x-ray scattering spectrum from diamond, normalized to the maximum of the elastic signal peak. Spectra were obtained by averaging over 18 000 shots using the x-ray beam in the SASE configuration along with a monochromator. The plasmon feature is presented on a linear scale in Fig. 2.

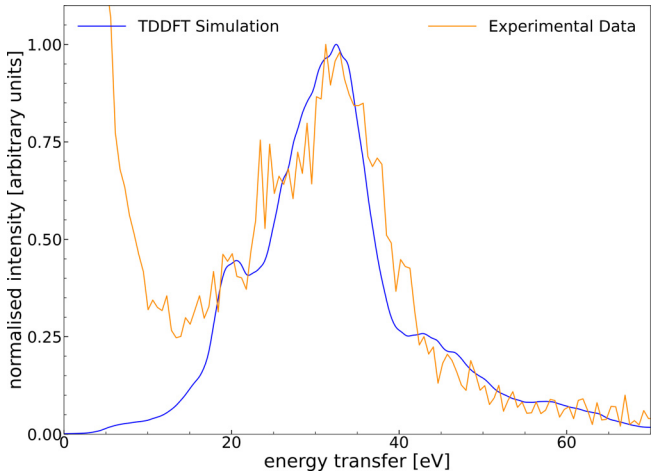

FIG. 2. Measured plasmon feature (orange) from Fig. 1 in comparison with the calculated plasmon feature (blue) after convolution with the instrument function.

high-pressure, high-temperature conditions. In previous experiments, polystyrene (CH) samples were dynamically compressed at the Linac Coherent Light Source showing C–H phase separation on nanosecond timescales using *in situ* x-ray diffraction.[24,57] Frydrych *et al.*[58] used a similar experimental setup to determine the degree of species separation in a dynamically compressed polystyrene sample to WDM conditions from spectrally resolved forward and backward x-ray scattering data. At pressures of the order of ∼150 GPa and temperatures around ∼6000 K, the carbon transforms into nanometer-sized diamonds. Measured diffraction lineouts provide indirect evidence for nearly complete C–H separation,[69] where the isolated hydrogen would be expected to be in a liquid metallic state. However, as XRD does not provide a signal from the weakly scattering hydrogen, and reflectivity measurements from the compression fronts remain elusive due to the ongoing chemical reaction,[59] so far there is no direct evidence for the presence of liquid metallic hydrogen in these experiments. Due to its sensitivity to electronic structure and bulk conductivity, the high-resolution forward scattering method described here can overcome these limitations and clarify the state of hydrogen in dynamically compressed C–H mixtures.

To test the sensitivity with the achieved spectral resolution, TDDFT calculations of the plasmon structures for C, H, and CH at conditions of $P \sim 150$ GPa and $T \sim 6000$ K were performed on ionic configurations obtained from density functional molecular dynamics (DFT-MD) simulations performed using VASP.[60–63] For consistency, the TDDFT calculations of the dynamic structure factor were performed at the k-vector magnitude of ∼0.94 Å^{-1}, i.e., the same as the forward scattering in the experiment. The spectral contributions of all three species were convolved with the experimentally obtained instrument function.[51] The results are depicted in Fig. 3 and show a single peak with an almost Gaussian shape for a fully mixed CH sample. For fully demixed CH, a culmination of two distinctly shifted plasmon features from the two separate components is observed, forming a double-peak structure. The peak at higher energy shifts originates from the collective excitations of the diamond valence band, while the peak at lower energy shifts represents the plasmon feature of liquid

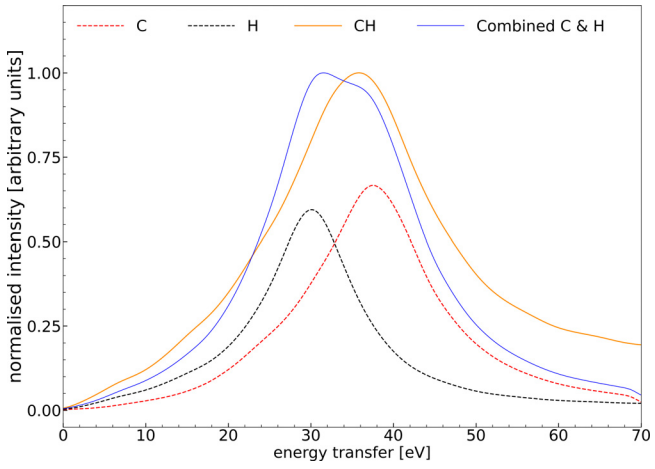

FIG. 3. Calculated spectra for CH in mixed state (orange) and demixed state (blue) for the scattering vector of $k = 0.94$ Å^{-1}. The demixed state plasmon is a combination of the characteristic carbon (red dotted) and metallic hydrogen (black dotted) features.

metallic hydrogen. With the experimentally demonstrated spectral resolution of ∼3 eV possible using the 40 μm HAPG crystals, and a separation between the peaks of ∼6–8 eV, C–H phase separation and hydrogen metallization can be observed using the demonstrated setup in future experiments adding a rep-rated drive laser.

Additional TDDFT dynamic structure factor calculations were performed on pure H and C, as well as other C–H mixtures (CH, CH_3, and C_3H) at different scattering vectors to obtain the respective plasmon peaks and plasmon dispersion shifts. Figure 4 shows the plasmon energy shifts for varying k-values for each species. The obtained results show that the separation between the features of the fully demixed components as shown in Fig. 3 is larger at smaller scattering

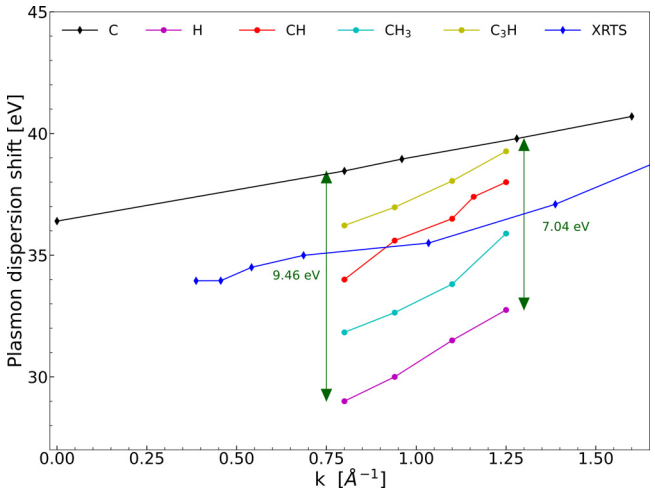

FIG. 4. Calculated plasmon energy shift for various species using the peak position of a respective plasmon in the forward scattering spectrum at different scattering vectors k. Plasmon shift in an experimental XRTS data at ambient conditions taken from Ref. 55 is also displayed for comparison.

vector magnitudes. The quadratic dispersion (shown up to $k \sim 1.60$) from the TDDFT results is weak, especially for carbon.[43,55] The remaining results exhibiting a slightly stronger quadratic dispersion are only shown for $k = 0.80$–$1.25\ \text{Å}^{-1}$ highlighting the spectral resolution in the plasmon peaks required for diagnostics. In addition, the dispersion feature obtained using XRTS[55] for diamond at ambient conditions is additionally shown for Ref. 55 highlighting the differences expected between ambient and warm dense carbon states. Thus, the corresponding experiments need to aim for small scattering angles and/or low photon energies to optimize the sensitivity for C–H separation and hydrogen metallization via inelastic x-ray scattering.

In conclusion, the described method using collective x-ray Thomson scattering is applicable to characterize liquid metallic hydrogen in the bulk of the sample, which is advantageous over the reflectivity measurements that can only probe the surface (which may be in a non-equilibrium state, e.g., a shock front). We presented how the exemplar scattering spectrum from ambient diamond recorded at the HED instrument of European XFEL agrees well with the TDDFT simulations performed. The existing resolution is capable of distinguishing the expected metallic hydrogen feature after demixing. In our demonstration experiment, ∼18 000 shots were accumulated due to a significant decrease in x-ray flux due to the usage of a monochromator. With the new possibility to use self-seeded x-ray beams providing a spectral resolution comparable to using the monochromator,[64] but with approximately 50 times more x-ray photons per pulse, the required number of shots will be significantly reduced. Moreover, the samples applied in the demonstration experiment were notably thinner than those in typical shock-compression experiments at XFEL sources (10 μm vs 50–100 μm). Therefore, it can be expected that an accumulation of approximately 1000 shots or even less is required to obtain the data quality presented here. While high repetition rates place high demands on target design and the target delivery system,[65] the corresponding developments are under way at the HED instrument, e.g., by allowing to replace targets without the need to break the vacuum in the interaction chamber.[66] Furthermore, plastics as a base target material allow for using tape samples that enable such rep-rated experiments with several 1000s of shots before targets have to be swapped.[67] Novel diagnostic tools combined with the new DiPOLE high-energy laser system at the HED instrument of EuXFEL will enable bulk-sensitive measurements of planetary core conditions. It is up to 10 Hz repetition rate, and pulse shaping capabilities[68] can be expected to play a crucial role in unlocking the physics behind the planets in the Solar System as well as the evolution of the steadily increasing number of confirmed exoplanets beyond.

ACKNOWLEDGMENTS

K.V., N.J.H., O.S.H., A.K.S., and D.K. were supported by the Helmholtz Association under VH-NG-1141, and O.S.H. was supported by the Helmholtz Association under Grant No. ERC-RA-0041. M.S. was supported by the Helmholtz Association under Grant No. VH-NG-1338. K.R. acknowledges funding by the Center for Advanced Systems Understanding (CASUS), which is financed by the German Federal Ministry of Education and Research (BMBF) and by the Saxon Ministry for Science, Culture and Tourism (SMWK) with tax funds on the basis of the budget approved by the Saxon State Parliament. The work of J.L. has been supported by GSI Helmholtzzentrum für Schwerionenforschung, Darmstadt as part of the R&D project GSI-URDK2224 with the University of Rostock. N.J.H. and L.B.F. acknowledge support from the Department of Energy, Office of Science, Office of Fusion Energy Sciences, under FWP 100182, and N.J.H. was supported by the Department of Energy, Laboratory Directed Research, and Development program at SLAC National Accelerator Laboratory, under Contract No. DE-AC02–76SF00515. The work of S.P.H-R. was performed under the auspices of the U.S. Department of Energy by Lawrence Livermore National Laboratory under Contract No. DEAC52-07NA27344. Z.H. and C.Q. acknowledge the financial support from the China Scholarship Council. The work of M.H. and A.A. is, in part, supported by the French Centre National de la Recherche Scientifique GoToXFEL program and it has also received funding from the European Research Council (ERC) under the European Union's Horizon 2020 research and innovation program (Grant Agreement No. 670787 D PLANETDIVE). The work of P.T.M. was supported by Deutsche Forschungsgemeinschaft (DFG – German Research Foundation) Project No. 505630685. S.S. was supported by DFG Project No. 495324226. Computations were performed on a Bull Cluster at the Center for Information Services and High-Performance Computing (ZIH) at Technische Universität Dresden and on the cluster Hemera at Helmholtz-Zentrum Dresden-Rossendorf (HZDR).

AUTHOR DECLARATIONS

Conflict of Interest

The authors have no conflicts to disclose.

Author Contributions

Divyanshu Ranjan: Formal analysis (equal); Investigation (equal); Methodology (equal); Resources (equal); Writing – original draft (equal); Writing – review & editing (equal). **Samuel Schumacher:** Validation (equal); Writing – review & editing (equal). **Philipp Thomas May:** Writing – review & editing (equal). **Alexis Amouretti:** Data curation (equal). **Karen Appel:** Data curation (equal). **Erik Brambrink:** Data curation (equal). **Valerio Cerantola:** Data curation (equal). **Deniza Chekrygina:** Data curation (equal). **Luke Bennett Fletcher:** Data curation (equal). **Sebastian Göde:** Data curation (equal). **Marion Harmand:** Data curation (equal). **Kushal ramakrishna:** Data curation (equal); Formal analysis (equal); Investigation (equal); Resources (equal); Validation (equal); Writing – review & editing (equal). **Nicholas J. Hartley:** Data curation (equal); Writing – review & editing (equal). **Stefan P. Hau-Riege:** Data curation (equal). **Mikako Makita:** Data curation (equal). **Alexander Pelka:** Data curation (equal). **Anja Katharina Schuster:** Data curation (equal). **Michal Šmíd:** Data curation (equal). **Toma Toncian:** Data curation (equal). **Min Zhang:** Data curation (equal); Resources (equal). **Thomas Robert Preston:** Data curation (equal); Writing – review & editing (equal). **Ulf Zastrau:** Data curation (equal). **Katja Voigt:** Data curation (equal); Methodology (equal); Resources (equal). **Jan Vorberger:** Formal analysis (equal); Resources (equal); Software (equal); Validation (equal); Writing – review & editing (equal). **Dominik Kraus:** Conceptualization (equal); Data curation (equal); Formal analysis (equal); Investigation (equal); Methodology (equal); Project administration (equal); Resources (equal); Supervision (equal); Validation (equal); Visualization (equal); Writing – review & editing (equal). **Oliver S. Humphries:** Data curation (equal); Methodology

(equal); Resources (equal); Software (equal); Validation (equal); Writing – review & editing (equal). **Benjamin Heuser:** Validation (equal); Writing – review & editing (equal). **Michael Gareth Stevenson:** Supervision (equal); Writing – review & editing (equal). **Julian Lütgert:** Validation (equal); Writing – review & editing (equal). **Zhiyu He:** Validation (equal); Writing – review & editing (equal). **Chongbing Qu:** Validation (equal); Writing – review & editing (equal).

DATA AVAILABILITY

The data that support the findings of this study are available from the corresponding authors upon reasonable request.

REFERENCES

[1]A. Wolszczan and D. A. Frail, "A planetary system around the millisecond pulsar PSR1257 + 12," Nature **355**, 145–147 (1992).
[2]M. Mayor and D. Queloz, "A Jupiter-mass companion to a solar-type star," Nature **378**, 355–359 (1995).
[3]See https://exoplanetarchive.ipac.caltech.edu/docs/counts_detail.html for "Exoplanet and Candidate Statistics, NASA Exoplanet Archive" (accessed March 20, 2022).
[4]See https://exoplanetarchive.ipac.caltech.edu/exoplanetplots/ for "Exoplanet Pre-Generated plots, NASA Exoplanet Archive" (accessed March 20, 2022).
[5]W. Borucki, "KEPLER Mission: Development and overview," Rep. Prog. Physics. **79**, 036901 (2016).
[6]T. Guillot, "Interiors of giant planets inside and outside the solar system," Science **286**, 72–77 (1999).
[7]R. Chau, S. Hamel, and W. Nellis, "Chemical processes in the deep interior of Uranus," Nat. Commun. **2**, 203 (2011).
[8]S. Lobanov, P. Chen, X.-J. Chen, C.-S. Zha, K. Litasov, and A. Goncharov, "Carbon precipitation from heavy hydrocarbon fluid in deep planetary interiors," Nat. Commun. **4**, 2446 (2013).
[9]F. Graziani, M. Desjarlais, R. Redmer, and S. Trickey, *Frontiers and Challenges in Warm Dense Matter* (Springer International Publishing, 2014).
[10]M. Bonitz, T. Dornheim, Z. A. Moldabekov, S. Zhang, P. Hamann, H. Kählert, A. Filinov, K. Ramakrishna, and J. Vorberger, "*Ab initio* simulation of warm dense matter," Phys. Plasmas **27**, 042710 (2020).
[11]E. Wigner and H. B. Huntington, "On the Possibility of a Metallic Modification of Hydrogen," J. Chem. Phys. **3**, 764–770 (1935).
[12]L. Landau and Y. B. Zeldovich, "On the relation between the liquid and the gaseous states of metals," Acta Physicochim. USSR **18**, 194–196 (1943).
[13]N. W. Ashcroft, "Metallic hydrogen: A high-temperature superconductor?," Phys. Rev. Lett. **21**, 1748–1749 (1968).
[14]S. A. Bonev, E. Schwegler, T. Ogitsu, and G. Galli, "A quantum fluid of metallic hydrogen suggested by first-principles calculations," Nature **431**, 669–672 (2004).
[15]V. E. Fortov, R. I. Ilkaev, V. A. Arinin, V. V. Burtzev, V. A. Golubev, I. L. Iosilevskiy, V. V. Khrustalev, A. L. Mikhailov, M. A. Mochalov, V. Y. Ternovoi, and M. V. Zhernokletov, "Phase transition in a strongly nonideal deuterium plasma generated by quasi-isentropical compression at megabar pressures," Phys. Rev. Lett. **99**, 185001 (2007).
[16]S. Scandolo, "Liquid–liquid phase transition in compressed hydrogen from first-principles simulations," Proc. Natl. Acad. Sci. U. S. A. **100**, 3051–3053 (2003).
[17]M. A. Morales, C. Pierleoni, E. Schwegler, and D. M. Ceperley, "Evidence for a first-order liquid-liquid transition in high-pressure hydrogen from ab initio simulations," Proc. Natl. Acad. Sci. U. S. A. **107**, 12799–12803 (2010).
[18]T. Guillot, "The interiors of giant planets: Models and outstanding questions," Annu. Rev. Earth Planet. Sci. **33**, 493–530 (2005).
[19]W. B. Hubbard, W. J. Nellis, A. C. Mitchell, N. C. Holmes, S. S. Limaye, and P. C. McCandless, "Interior structure of Neptune: Comparison with Uranus," Science **253**, 648–651 (1991).
[20]R. Helled, J. D. Anderson, M. Podolak, and G. Schubert, "Interior models of Uranus and Neptune," Astrophys. J. **726**, 15 (2010).
[21]N. Nettelmann, K. Wang, J. Fortney, S. Hamel, S. Yellamilli, M. Bethkenhagen, and R. Redmer, "Uranus evolution models with simple thermal boundary layers," Icarus **275**, 107–116 (2016).
[22]H. Hirai, K. Konagai, T. Kawamura, Y. Yamamoto, and T. Yagi, "Polymerization and diamond formation from melting methane and their implications in ice layer of giant planets," Phys. Earth Planet. Inter. **174**, 242–246 (2009).
[23]M. Ross, "The ice layer in Uranus and Neptune-diamonds in the sky?," Nature **292**, 435–436 (1981).
[24]D. Kraus, N. Hartley, S. Frydrych, A. Schuster, K. Rohatsch, M. Rödel, T. Cowan, S. Brown, E. Cunningham, T. Driel, L. Fletcher, E. Galtier, E. Gamboa, A. Laso Garcia, D. Gericke, E. Granados, P. Heimann, H. Lee, M. MacDonald, and J. Vorberger, "High-pressure chemistry of hydrocarbons relevant to planetary interiors and inertial confinement fusion," Phys. Plasmas **25**, 056313 (2018).
[25]L. Benedetti, J. Nguyen, W. Caldwell, H. Liu, M. Kruger, and R. Jeanloz, "Dissociation of CH_4 at high pressures and temperatures: Diamond formation in giant planet interiors?," Science **286**, 100–102 (1999).
[26]Z. He, M. Rödel, J. Lütgert, A. Bergermann, M. Bethkenhagen, D. Chekrygina, T. E. Cowan, A. Descamps, M. French, E. Galtier, A. E. Gleason, G. D. Glenn, S. H. Glenzer, Y. Inubushi, N. J. Hartley, J.-A. Hernandez, B. Heuser, O. S. Humphries, N. Kamimura, K. Katagiri, D. Khaghani, H. J. Lee, E. E. McBride, K. Miyanishi, B. Nagler, B. Ofori-Okai, N. Ozaki, S. Pandolfi, C. Qu, D. Ranjan, R. Redmer, C. Schoenwaelder, A. K. Schuster, M. G. Stevenson, K. Sueda, T. Togashi, T. Vinci, K. Voigt, J. Vorberger, M. Yabashi, T. Yabuuchi, L. M. V. Zinta, A. Ravasio, and D. Kraus, "Diamond formation kinetics in shock-compressed C—H—O samples recorded by small-angle x-ray scattering and x-ray diffraction," Sci. Adv. **8**, eabo0617 (2022).
[27]M. Murillo, "Strongly coupled plasma physics and high energy-density matter," Phys. Plasmas **11**, 2964–2971 (2004).
[28]D. Riley, "Generation and characterisation of warm dense matter with intense lasers," Plasma Phys. Controlled Fusion **60**, 1–11 (2017).
[29]M. Eremets and I. Troyan, "Conductive dense hydrogen," Nat. Mater. **10**, 927–931 (2011).
[30]R. P. Dias and I. F. Silvera, "Observation of the Wigner-Huntington transition to metallic hydrogen," Science **355**, 715–718 (2017).
[31]I. F. Silvera, R. Dias, O. Noked, A. Salamat, and M. Zaghoo, "Metallic hydrogen," J. Low Temp. Phys. **187**, 4–19 (2017).
[32]P. Loubeyre, F. Occelli, and P. Dumas, "Synchrotron infrared spectroscopic evidence of the probable transition to metal hydrogen," Nature **577**, 631–635 (2020).
[33]M. Knudson, M. Desjarlais, A. Becker, R. Lemke, K. Cochrane, M. Savage, D. Bliss, T. Mattsson, and R. Redmer, "High-pressure physics. Direct observation of an abrupt insulator-to-metal transition in dense liquid deuterium," Science **348**, 1455–1460 (2015).
[34]P. Celliers, M. Millot, S. Brygoo, R. Mcwilliams, D. Fratanduono, J. Rygg, A. Goncharov, P. Loubeyre, J. Eggert, L. Peterson, N. Meezan, S. Pape, G. Collins, R. Jeanloz, and R. Hemley, "Insulator-metal transition in dense fluid deuterium," Science **361**, 677–682 (2018).
[35]S. Weir, A. Mitchell, and W. Nellis, "Metallization of Fluid Molecular Hydrogen at 140 GPa (1.4 Mbar)," Phys. Rev. Lett. **76**, 1860–1863 (1996).
[36]P. Davis, T. Döppner, J. Rygg, C. Fortmann, L. Divol, A. Pak, L. Fletcher, A. Becker, B. Holst, P. Sperling, R. Redmer, M. Desjarlais, P. Celliers, G. Collins, O. Landen, R. Falcone, and S. Glenzer, "X-ray scattering measurements of dissociation-induced metallization of dynamically compressed deuterium," Nat. Commun. **7**, 11189 (2016).
[37]P. Sperling, E. Gamboa, H. Lee, H. Chung, E. Galtier, Y. Omarbakiyeva, H. Reinholz, G. Roepke, U. Zastrau, J. Hastings, L. Fletcher, and S. Glenzer, "Free-electron x-ray laser measurements of collisional-damped plasmons in isochorically heated warm dense matter," Phys. Rev. Lett. **115**, 115001 (2015).
[38]M. Marques and E. Gross, "Time-dependent density functional theory," Annu. Rev. Phys. Chem. **55**, 427–455 (2004).
[39]A. Kritcher, P. Neumayer, H. Lee, T. Döppner, R. Falcone, S. Glenzer, and E. Morse, "Demonstration of x-ray Thomson scattering using picosecond k-α x-ray sources in the characterization of dense heated matter," Rev. Sci. Instrum. **79**, 10E739 – 10E739 (2008).

[40]S. H. Glenzer, W. Rozmus, B. J. MacGowan, K. G. Estabrook, J. D. D. Groot, G. B. Zimmerman, H. A. Baldis, J. A. Harte, R. W. Lee, E. A. Williams, and B. G. Wilson, "Thomson scattering from high-Z laser-produced plasmas," Phys. Rev. Lett. **82**, 97–100 (1999).
[41]S. H. Glenzer and R. Redmer, "X-ray Thomson scattering in high energy density plasmas," Rev. Mod. Phys. **81**, 1625–1663 (2009).
[42]R. Kubo, "The fluctuation-dissipation theorem," Rep. Prog. Phys. **29**, 255 (1966).
[43]K. Ramakrishna and J. Vorberger, "Ab initio dielectric response function of diamond and other relevant high pressure phases of carbon," J. Phys.: Condens. Matter **32**, 095401 (2019).
[44]See http://elk.sourceforge.net/ for "ELK, all-electron full-potential linearised augmented plane wave (FP-LAPW) code" (2022).
[45]S. Sharma, J. Dewhurst, A. Sanna, and E. Gross, "Bootstrap approximation for the exchange-correlation kernel of time-dependent density-functional theory," Phys. Rev. Lett. **107**, 186401 (2011).
[46]A. Marini, C. Hogan, M. Gruening, and D. Varsano, "yambo: An ab initio tool for excited state calculations," Comput. Phys. Commun. **180**, 1392–1403 (2009).
[47]W. Kohn and L. J. Sham, "Self-consistent equations including exchange and correlation effects," Phys. Rev. **140**, A1133–A1138 (1965).
[48]P. Giannozzi, O. Andreussi, T. Brumme, O. Bunau, M. B. Nardelli, M. Calandra, R. Car, C. Cavazzoni, D. Ceresoli, M. Cococcioni *et al.*, "Advanced capabilities for materials modelling with Quantum ESPRESSO," J. Phys. Matter **29**, 465901 (2017).
[49]J. P. Perdew, K. Burke, and M. Ernzerhof, "Generalized gradient approximation made simple," Phys. Rev. Lett. **77**, 3865 (1996).
[50]M. Nakatsutsumi, K. Appel, G. Priebe, I. Thorpe, A. Pelka, B. Muller, and T. Tschentscher, "Scientific Instrument High Energy Density Physics (HED)," European XFEL Technical Report No. 1–196 (2014).
[51]K. Voigt, M. Zhang, K. Ramakrishna, A. Amouretti, K. Appel, E. Brambrink, V. Cerantola, D. Chekrygina, T. Döppner, R. Falcone, K. Falk, L. Fletcher, D. Gericke, S. Göde, M. Harmand, N. Hartley, S. Hau-Riege, L.-G. Huang, O. Humphries, and D. Kraus, "Demonstration of an x-ray Raman spectroscopy setup to study warm dense carbon at the high energy density instrument of European XFEL," Phys. Plasmas **28**, 082701 (2021).
[52]T. Preston, S. Göde, J.-P. Schwinkendorf, K. Appel, E. Brambrink, V. Cerantola, H. Höppner, M. Makita, A. Pelka, C. Prescher, K. Sukharnikov, A. Schmidt, I. Thorpe, T. Toncian, A. Amouretti, D. Chekrygina, R. Falcone, K. Falk, L. Fletcher, E. Galtier, M. Harmand, N. Hartley, S. Hau-Riege, P. Heimann, L. Huang, O. Humphries, O. Karnbach, D. Kraus, H. Lee, B. Nagler, S. Ren, A. Schuster, M. Smid, K. Voigt, M. Zhang, and U. Zastrau, "Design and performance characterisation of the HAPG von Hámos spectrometer at the high energy density instrument of the European XFEL," J. Instrumentation **15**, P11033 (2020).
[53]A. Mozzanica, A. Bergamaschi, M. Brueckner, S. Cartier, R. Dinapoli, D. Greiffenberg, J. Jungmann-Smith, D. Maliakal, D. Mezza, M. Ramilli, C. Ruder, L. Schaedler, B. Schmitt, X. Shi, and G. Tinti, "Characterization results of the JUNGFRAU full scale readout ASIC," J. Instrumentation **11**, C02047–C02047 (2016).
[54]K. Nishimura, G. Blaj, P. Caragiulo, G. Carini, A. Dragone, G. Haller, P. Hart, J. Hasi, R. Herbst, S. Herrmann, C. Kenney, M. Kwiatkowski, B. Markovic, S. Osier, J. Pines, B. Reese, J. Segal, A. Tomada, and M. Weaver, "Design and performance of the ePix camera system," AIP Conf. Proc. **1741**, 040047 (2016).
[55]E. Gamboa, L. Fletcher, H. Lee, M. MacDonald, U. Zastrau, M. Gauthier, D. Gericke, J. Vorberger, E. Granados, J. Hastings *et al.*, "Band gap opening in strongly compressed diamond observed by x-ray energy loss spectroscopy," Technical Report No. SLAC-PUB-16488 (SLAC National Accelerator Laboratory, Menlo Park, CA, 2016).
[56]L. Bursill, J. Peng, and S. Prawer, "Plasmon response and structure of nanocrystalline diamond powder," Philos. Mag. A **76**, 769–781 (1997).
[57]D. Kraus, J. Vorberger, A. Pak, N. Hartley, L. Fletcher, S. Frydrych, E. Galtier, E. Gamboa, D. Gericke, S. Glenzer, E. Granados, M. MacDonald, A. Mackinnon, E. McBride, I. Nam, P. Neumayer, M. Roth, A. Saunders, A. Schuster, and R. Falcone, "Formation of diamonds in laser-compressed hydrocarbons at planetary interior conditions," Nat. Astron. **1**, 606–611 (2017).
[58]S. Frydrych, J. Vorberger, N. Hartley, A. Schuster, K. Ramakrishna, A. Saunders, T. van Driel, R. Falcone, L. Fletcher, E. Galtier *et al.*, "Demonstration of x-ray Thomson scattering as diagnostics for miscibility in warm dense matter," Nat. Commun. **11**, 2620 (2020).
[59]N. Hartley, C. Zhang, X. Duan, L.-G. Huang, S. Jiang, Y. Li, L. Yang, A. Pelka, Z. Wang, J. Yang, and D. Kraus, "Dynamically pre-compressed hydrocarbons studied by self-impedance mismatch," Matter Radiat. Extremes **5**, 028401 (2020).
[60]G. Kresse and J. Hafner, "*Ab initio* molecular dynamics for liquid metals," Phys. Rev. B **47**, 558–561 (1993).
[61]G. Kresse and D. Joubert, "From ultrasoft pseudopotentials to the projector augmented-wave method," Phys. Rev. B **59**, 1758–1775 (1999).
[62]G. Kresse and J. Furthmüller, "Efficiency of *ab-initio* total energy calculations for metals and semiconductors using a plane-wave basis set," Comput. Mater. Sci. **6**, 15–50 (1996).
[63]G. Kresse and J. Furthmüller, "Efficient iterative schemes for ab initio total-energy calculations using a plane-wave basis set," Phys. Rev. B **54**, 11169–11186 (1996).
[64]J. Amann, W. Berg, V. Blank, F. J. Decker, Y. Ding, P. Emma, Y. Feng, J. Frisch, D. Fritz, J. Hastings, Z. Huang, J. Krzywinski, R. Lindberg, H. Loos, A. Lutman, H. D. Nuhn, D. Ratner, J. Rzepiela, D. Shu, Y. Shvyd'Ko, S. Spampinati, S. Stoupin, S. Terentyev, E. Trakhtenberg, D. Walz, J. Welch, J. Wu, A. Zholents, and D. Zhu, "Demonstration of self-seeding in a hard-x-ray free-electron laser," Nat. Photonics **6**, 693–698 (2012).
[65]I. Prencipe, J. Fuchs, S. Pascarelli, D. W. Schumacher, R. B. Stephens, N. B. Alexander, R. Briggs, M. Büscher, M. O. Cernaianu, A. Choukourov *et al.*, "Targets for high repetition rate laser facilities: Needs, challenges and perspectives," High Power Laser Sci. Eng. **5**, e17 (2017).
[66]U. Zastrau, K. Appel, C. Baehtz, O. Baehr, L. Batchelor, A. Berghäuser, M. Banjafar, E. Brambrink, V. Cerantola, T. E. Cowan, H. Damker, S. Dietrich, S. Di Dio Cafiso, J. Dreyer, H.-O. Engel, T. Feldmann, S. Findeisen, M. Foese, D. Fulla-Marsa, S. Göde, M. Hassan, J. Hauser, T. Herrmannsdörfer, H. Höppner, J. Kaa, P. Kaever, K. Knöfel, Z. Konôpková, A. Laso García, H.-P. Liermann, J. Mainberger, M. Makita, E.-C. Martens, E. E. McBride, D. Möller, M. Nakatsutsumi, A. Pelka, C. Plueckthun, C. Prescher, T. R. Preston, M. Röper, A. Schmidt, W. Seidel, J.-P. Schwinkendorf, M. O. Schoelmerich, U. Schramm, A. Schropp, C. Strohm, K. Sukharnikov, P. Talkovski, I. Thorpe, M. Toncian, T. Toncian, L. Wollenweber, S. Yamamoto, and T. Tschentscher, "The high energy density scientific instrument at the European XFEL," J. Synchrotron Radiat. **28**, 1393–1416 (2021).
[67]F. P. Condamine, N. Jourdain, J.-C. Hernandez, M. Taylor, H. Bohlin, A. Fajstavr, T. M. Jeong, D. Kumar, T. Laštovička, O. Renner, and S. Weber, "High-repetition rate solid target delivery system for PW-class laser-matter interaction at ELI Beamlines," Rev. Sci. Instrum. **92**, 063504 (2021).
[68]S. Banerjee, K. Ertel, P. D. Mason, P. J. Phillips, M. D. Vido, J. M. Smith, T. J. Butcher, C. Hernandez-Gomez, R. J. S. Greenhalgh, and J. L. Collier, "DiPOLE: A 10 J, 10 Hz cryogenic gas cooled multi-slab nanosecond Yb:YAG laser," Opt. Express **23**, 19542–19551 (2015).
[69]D. Kraus, J. Vorberger, N. J. Hartley, J. Lütgert, M. Rödel, D. Chekrygina, T. Döppner, T. van Driel, R. W. Falcone, L. B. Fletcher, S. Frydrych, E. Galtier, D. O. Gericke, S. H. Glenzer, E. Granados, Y. Inubushi, N. Kamimura, K. Katagiri, M. J. MacDonald, A. J. MacKinnon, T. Matsuoka, K. Miyanishi, E. E. McBride, I. Nam, P. Neumayer, N. Ozaki, A. Pak, A. Ravasio, A. M. Saunders, A. K. Schuster, M. G. Stevenson, K. Sueda, P. Sun, T. Togashi, K. Voigt, M. Yabashi, and T. Yabuuchi, "Indirect evidence for elemental hydrogen in laser-compressed hydrocarbons," Phys. Rev. Res. **5**, L022023 (2023).